Supplementary Information: Spinon Fermi surface spin liquid in a triangular lattice antiferromagnet $NaYbSe_2$

Peng-Ling Dai[#],[1] Gaoning Zhang[#],[2] Yaofeng Xie,[3] Chunruo Duan,[3] Yonghao Gao,[4] Zihao Zhu,[4] Erxi Feng,[5] Chien-Lung Huang,[3] Huibo Cao,[5] Andrey Podlesnyak,[5] Garrett E. Granroth,[5] Michelle S. Everett,[5] Joerg C. Neuefeind,[5] David Voneshen,[6,7] Shun Wang,[8] Guotai Tan,[1] Emilia Morosan,[3] Xia Wang,[2] Lei Shu,[4] Gang Chen,[9,4,*] Yanfeng Guo,[2,†] Xingye Lu,[1,‡] and Pengcheng Dai[3,§]

[1] *Center for Advanced Quantum Studies and Department of Physics, Beijing Normal University, Beijing 100875, China*
[2] *School of Physical Science and Technology, ShanghaiTech University, Shanghai 201210, China*
[3] *Department of Physics and Astronomy, Rice University, Houston, TX 77005, USA*
[4] *State Key Laboratory of Surface Physics, Department of Physics, Fudan University, Shanghai 200433, China*
[5] *Neutron Scattering Division, Oak Ridge National Laboratory, Oak Ridge, TN 37831*
[6] *ISIS Facility, Rutherford Appleton Laboratory, Chilton, Didcot, Oxfordshire OX11 0QX, UK*
[7] *Department of Physics, Royal Holloway University of London, Egham, TW20 0EX, UK*
[8] *School of Physics, Huazhong University of Science and Technology, Wuhan 430074, China*
[9] *Department of Physics and HKU-UCAS Joint Institute for Theoretical and Computational Physics at Hong Kong, The University of Hong Kong, Hong Kong, China*

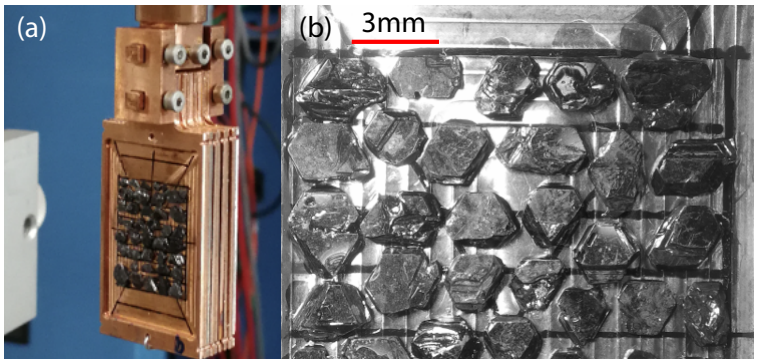


FIG. 1. **Aligned $NaYbSe_2$ single crystals for time-of-flight neutron scattering experiments.** (a) $NaYbSe_2$ single crystals are glued on oxygen-free copper sample holder using CYTOP M-type glue, and then attached onto the cold tip of a dilute refrigerator. (b) Zoomed-in view of the sample area. The self-cleaving edges are along the $[1, 1, 0]$ direction. The mosaic for (003) nuclear peak in [HHL] plane is $\sim 10.4^\circ$ (FWHM), and for (-110) in [HK0] plane $\sim 6.7^\circ$.

$NaYbSe_2$	X-ray refinement
$\mathbf{a} = \mathbf{b}$ (Å)	4.0609(1)
$\mathbf{c}$ (Å)	20.7425(1)
Total reflections	1334
Unique reflections	238 ($I > 2\sigma$)
Extinction	0.000639
R_F^2(%)	5.57
$R_F^2 w$(%)	8.14
R_F(%)	3.07
χ^2	2.42
Temperature (K)	250

Atoms	z	Occ.	U	site	symmetry
Na1	0.5	0.952(10)	0.013(4)	3*b*	-3m
Yb2	0.5	0.048(10)	0.013(4)	3*b*	-3m
Yb1	0	1.000	0.0092(5)	3*a*	-3m
Se1	0.2572(1)	1.000(2)	0.0094(10)	6*c*	3m
Te1	0.2572(1)	0.000(2)	0.0094(10)	6*c*	3m

Anisotropic displacement parameters (Å^2)				
Atoms	$U_{11} = U_{22}$	U_{33}	U_{12}	$U_{13} = U_{23}$
Na1	0.015(4)	0.011(4)	0.007(4)	0
Yb2	0.015(4)	0.011(4)	0.007(4)	0
Yb1	0.0074(5)	0.0129(5)	0.0037(5)	0
Se1	0.0088(10)	0.0108(10)	0.0044(10)	0
Te1	0.0088(10)	0.0108(10)	0.0044(10)	0

TABLE I. **Results of X-ray single crystal refinement for $NaYbSe_2$ ($R\bar{3}m$).** The structural parameters of $NaYbSe_2$ measured at 250 K by X-ray diffraction using a Rigaku XtaLAB PRO diffractometer at Spallation Neutron Source, ORNL. Atomic positions are Na1: Na (0, 0, 0.5); Yb1: Yb (0, 0, 0); Se1: Se (0, 0, 0.2572). In our fitting model, certain amount of Yb (Yb2) is allow to occupy Na1 sites, and some Te1 could replace Se1. X-rays are particularly sensitive to site mixing between Na (Se) and Yb (Te), as they have significantly different atomic electron numbers. The best fitting generates $4.8\% \pm 1\%$ occupancy (Occ.) of the Na1 sites by Yb2 and shows the absence of Te1 in the Se1 sites. Atomic displacement parameters U have units of Å^2. Non-zero U elements are listed in the table. The calculated structural factor F^2 and its comparison with observed F^2 are shown in Fig. 1(f) of the main text.

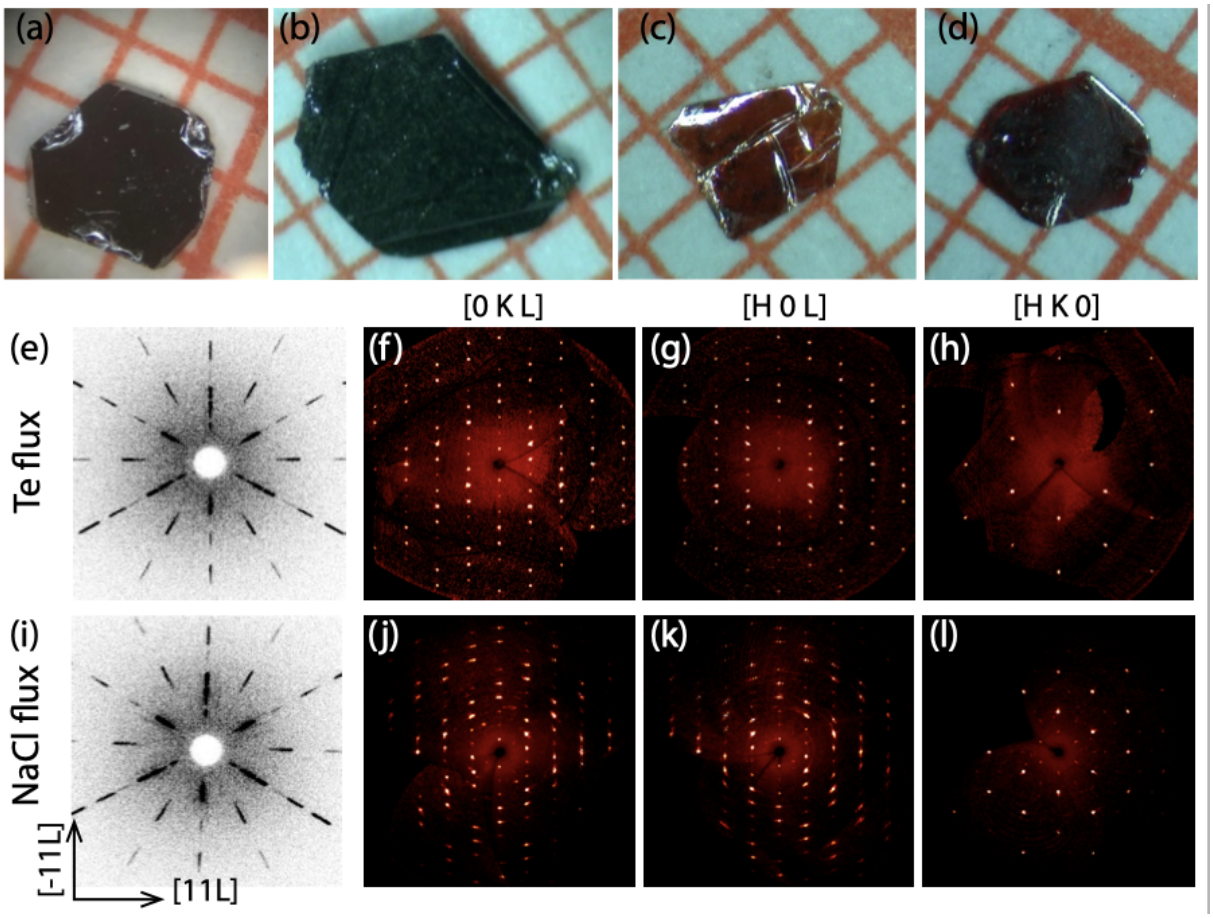


FIG. 2. **Morphology and x-ray diffraction of $NaYbSe_2$ crystals grown by different flux.** $NaYbSe_2$ single crystals grown with Te (a), (b) and NaCl (c), (d) as the flux. (e) Laue pattern and (f-h) single crystal x-ray diffraction results for the crystals grown with Te as the flux. (i-l) Laue and single crystal x-ray diffraction results for the crystals grown with NaCl as the flux.

SPECIFIC HEAT

Regarding the temperature dependence of specific heat and its connection to the ground state of the QSL, several remarks are in line.

1. For spinon Fermi surface alone, one merely has a $C_v \propto T$ behavior. For a $U(1)$ QSL, $C_v \propto T^{2/3}$ is the result when one includes the $U(1)$ gauge fluctuation on top of the spinon Fermi surface. In reality, it is unclear for a physical system at what temperature this gauge fluctuation starts to become important and modify the low temperature behavior. In $YbMgGaO_4$, if this is due to gauge fluctuation, then the gauge fluctuation appears at the measured temperature window. If gauge fluctuation appears at much lower temperatures, the specific heat would behave mostly as $C_v \propto T$ in the measured temperature range.

2. If the $U(1)$ gauge is higgsed down to Z_2 gauge at low energies by (weak) spinon pairing while the Fermi surface/pocket is preserved, one would not need to worry about the low energy gauge fluctuations and we have $C_v \propto T$.

This is the reason that we claimed spinon Fermi surface state and did not emphasize the $U(1)$ QSL. Maybe it is also worthwhile and instructive for us to mention the old works and proposed understanding about organic spin liquids. In fact, the κ-ET organic spin liquid also had $C_v \propto T$ [**?**], despite it was proposed as a spinon Fermi surface $U(1)$ spin liquid [at least as a parent starting state]. To reconcile $U(1)$ QSL with $C_v \propto T$ and other anomalies at low temperatures, Patrick Lee and SungSik Lee later proposed the idea of Amperean pairing mechanism that gaps out the continuous gauge but keeps the Fermi surface/pocket [**?**].

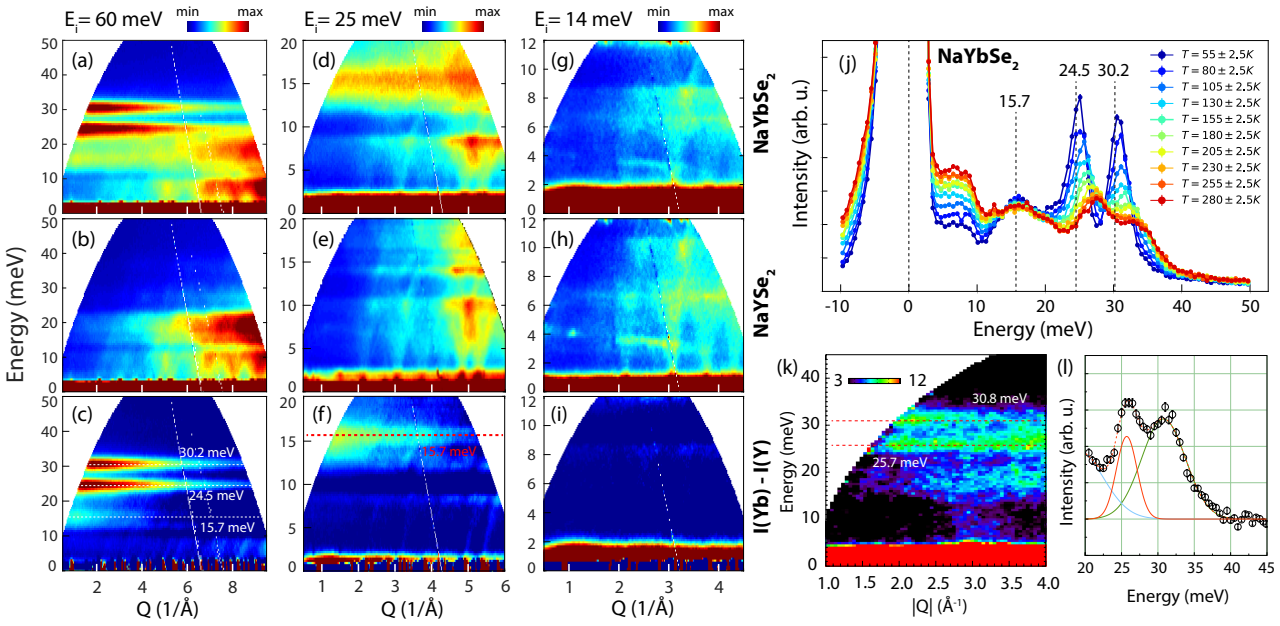


FIG. 3. **Crystal electric field (CEF) excitations in $NaYbSe_2$.** (a)-(j) CEF excitations of polycrystalline $NaYbSe_2$ sample measured at $T = 13$ K with $E_i = 60$, 25, and 14 meV. (k),(l) CEF excitations observed in $NaYbSe_2$ single crystals at $T = 40$ mK. Neutron scattering intensity measured on (a), (d), (g) $NaYbSe_2$, and (b), (e), (h) non-magnetic $NaYSe_2$. (c), (f), (g) Intensity difference between $NaYbSe_2$ and $NaYSe_2$. Three CEF excitation levels (white and red dashed lines) with $E = 15.7, 24.5$ and 30.2 meV at $T = 13$ K are identified. (j) Temperature dependence of energy cuts measured with E_i=60 meV. The three CEF excitations decrease in intensity and the two higher branches shift to higher energies with increasing temperature, which has been attributed to CEF-phonon coupling as reported in ref. [**?**]. (k) Neutron scattering intensity colormap for the $NaYbSe_2$ single crystal sample set (with a total mass of 3.7 grams). Two non-dispersive excitation branches with $E \approx 25.7$ and 30.8 meV can be identified as the two higher CEF excitations. (l) Energy cut with $|Q| = [1, 4]$ Å^{-1} extracted from (k) shows the two CEF excitation peaks.

* gangchen.physics@gmail.com
† guoyf@shanghaitech.edu.cn
‡ luxy@bnu.edu.cn
§ pdai@rice.edu

[1] Zhang, Z. *et al.* Crystalline Electric-Field Excitations in Quantum Spin Liquids Candidate $NaYbSe_2$. arXiv:2002.04772.
[2] Yamashita, S. *et al.* Thermodynamic properties of a spin-1/2 spin-liquid state in a κ-type organic salt. Nature Physics **4**, 459 (2008).
[3] Lee, S. *et al.* Amperean Pairing Instability in the $U(1)$ Spin Liquid State with Fermi Surface and Application to κ-(BEDT-TTFE)$_2$Cu$_2$CN$_3$. Phys. Rev. Lett. **98**, 067006 (2007).

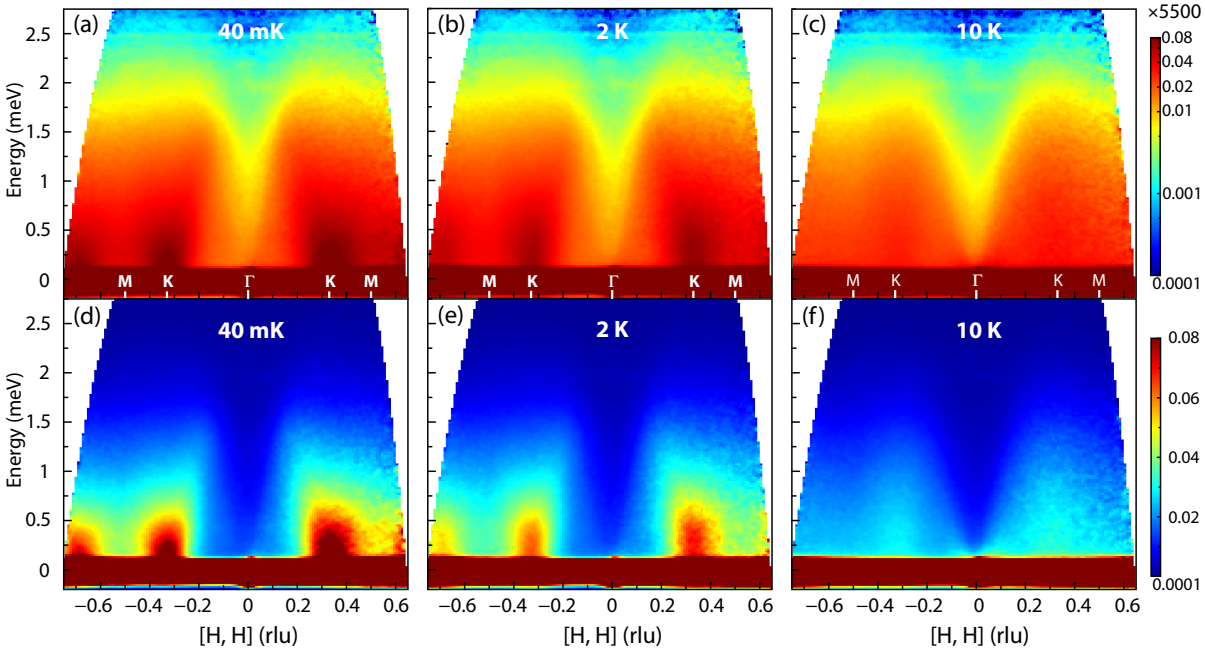


FIG. 4. **Temperature- and momentum-dependent magnetic excitation spectra along the high symmetry directions** $K_2 - M_2 - K_1 - \Gamma_1$. (a)-(c) are plotted in logarithmic scale and show the continuum clearly. (d)-(e) are plotted in linear scale with the same intensity range, emphasizing the enhancement of the spectral weight at the K points. The data were collected with $E_i = 3.32$ meV and $k_i \parallel [H, H, L]$.

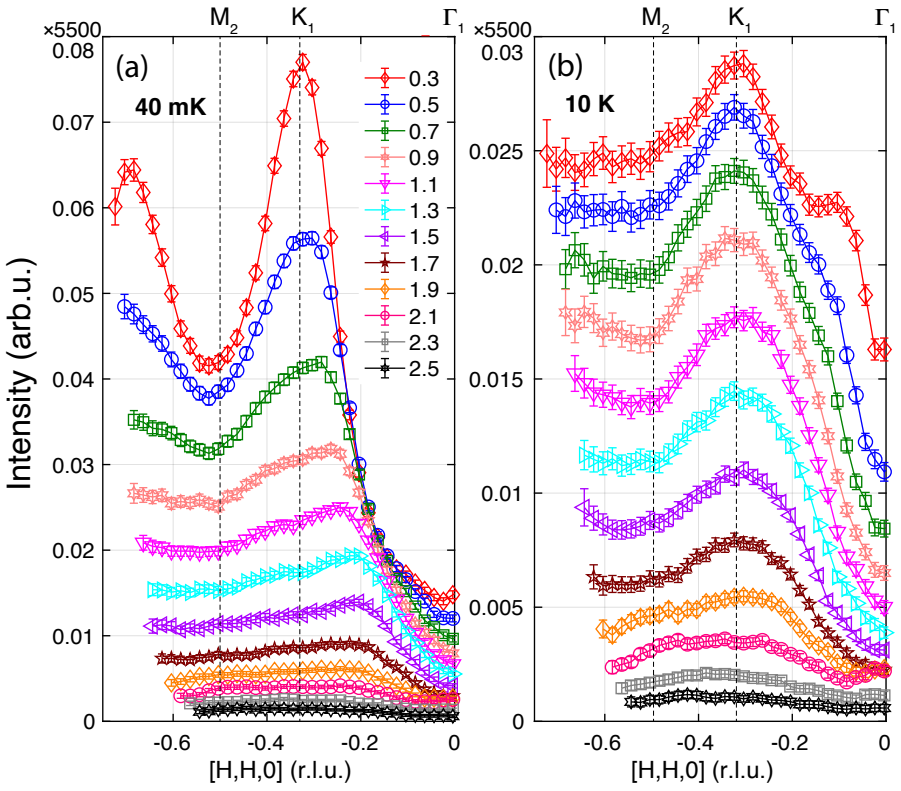


FIG. 5. **Constant-energy one dimensional cuts along the** $K_2 - M_2 - K_1 - \Gamma_1$ **direction**. The cuts are extracted from the colormaps in Fig. 4, with energies $E = 0.3 \pm 0.1, ..., 2.5 \pm 0.1$ meV.

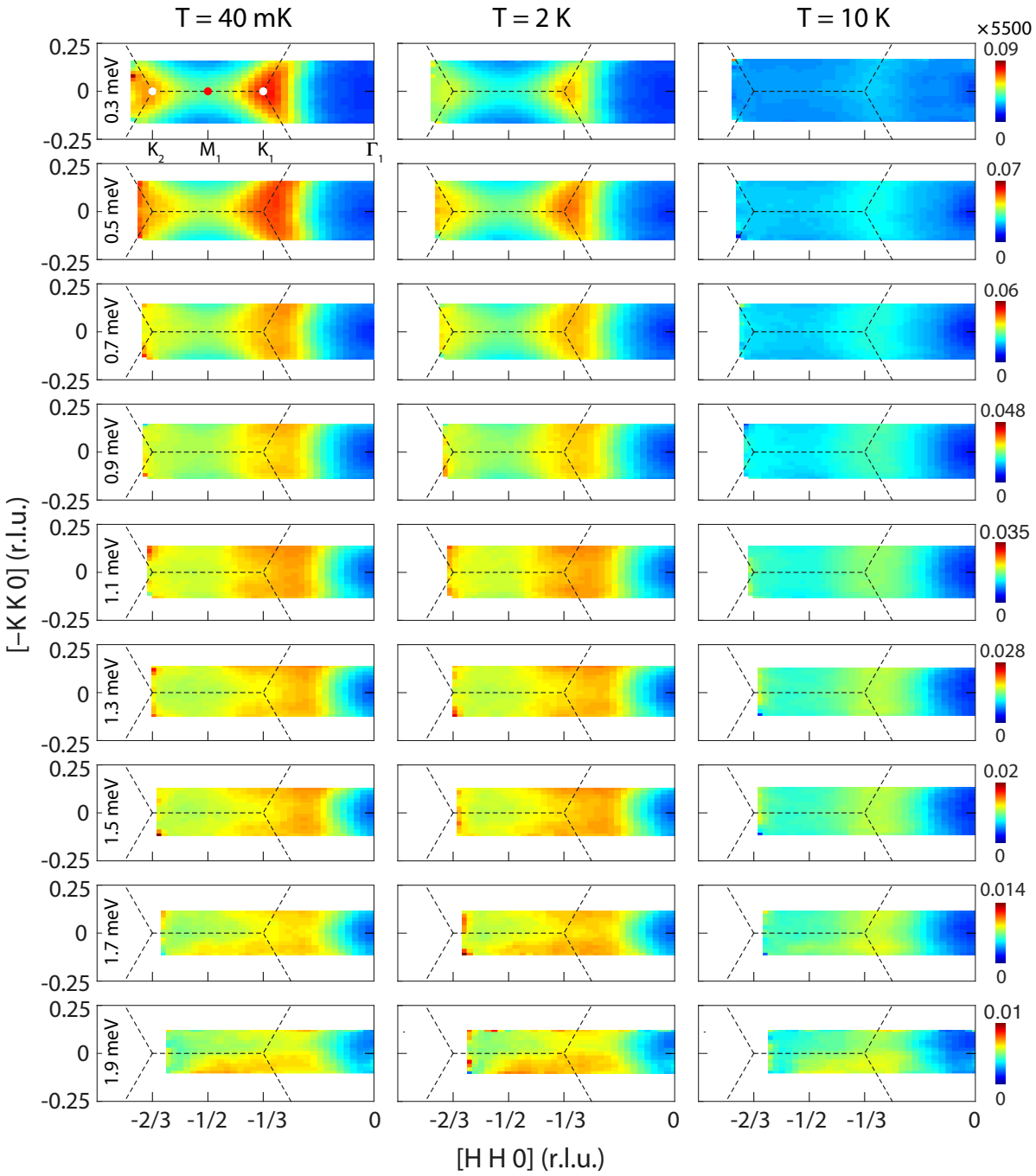


FIG. 6. **Constant energy slices of magnetic excitations in the $[H, K]$ plane measured with $k_i \parallel [H, H, L]$.** The data were collected with $E_i = 3.32$ meV at $T = 40$ mK, 2K, and 10K.

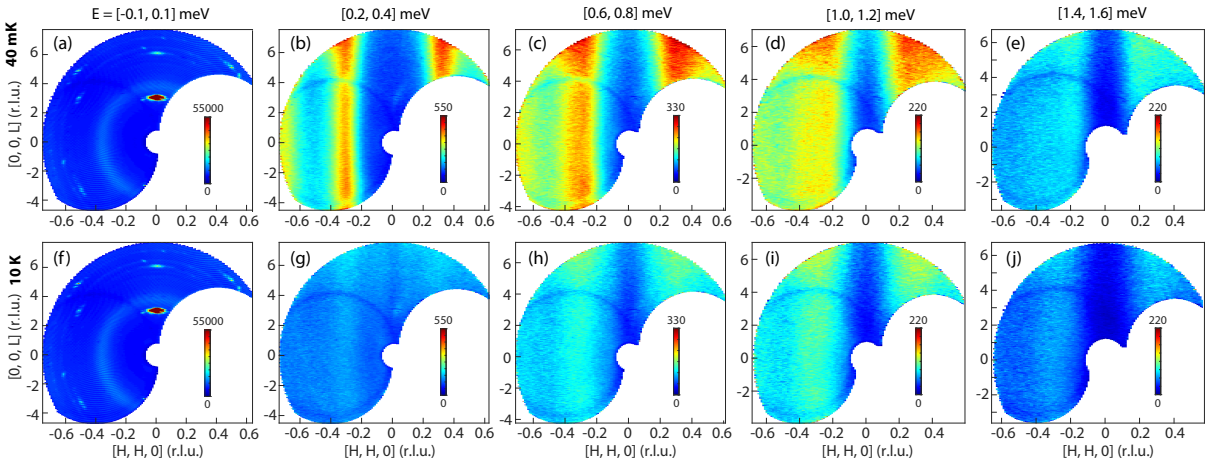


FIG. 7. **Constant energy slices of magnetic excitations in the $[H, H, L]$ plane measured with $k_i \parallel [H, H, L]$.** The data were collected with $E_i = 3.32$ meV at $T = 40$ mK (a)-(e) and 10 K (f)-(j).

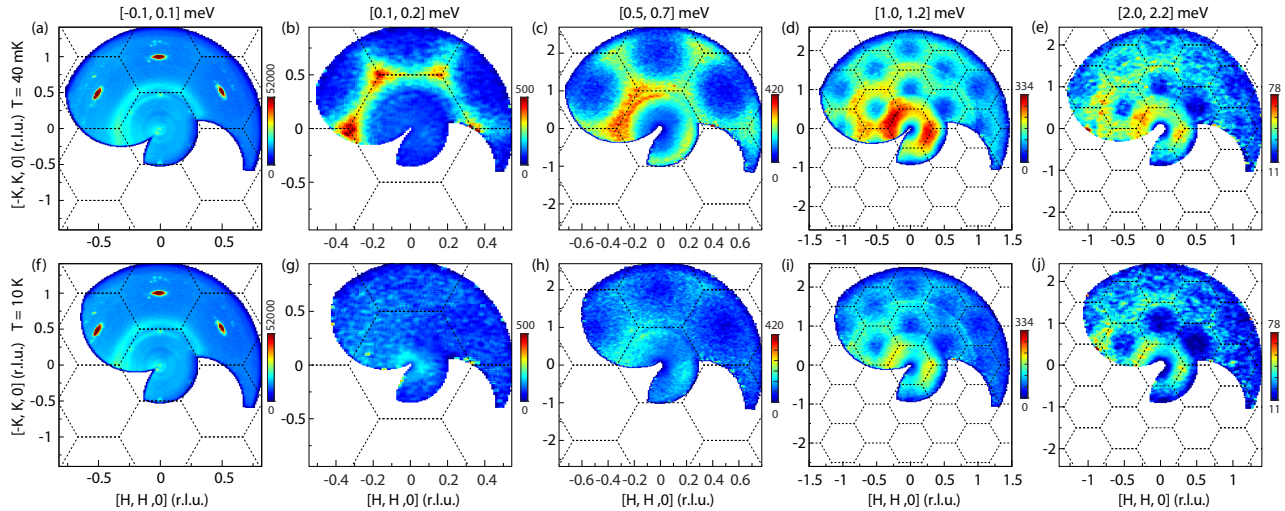


FIG. 8. **Constant energy slices of magnetic excitations in the $[H, K]$ plane measured with $k_i \parallel [H, K, 0]$.** The data were collected with $E_i = 3.70$ meV at $T = 40$ mK and 10K. The slices (a) and (f) are raw data for the symmetrized slice in Fig. 2(b) of the main text. (b)-(e) and (g)-(j) corresponds to the symmetrized slices in the Fig. 3 of the main text. Note that the background is anisotropic, as can be seen from the incoherent scattering close to the zone boundary of the first Brillouin zone in (a) and (f). In (a) and (f), the equivalent nuclear Bragg peaks $(0, -1, 0)$, $(-1, 1, 0)$, $(0, 1, 0)$ are not identical in intensity. $(0, -1, 0)$ and $(-1, 1, 0)$ are stronger than $(0, 1, 0)$. Since the samples are glued onto a rectangle area 15×20 mm^2, and the beam width is about 20 mm, the whole sample volume was not always in the beam during the sample rotational angular range of 180°. This can explain the intensity differences between the three equivalent nuclear Bragg peaks. The anisotropic incoherent scattering could arise from the sample holder which contains a 4 mm^3 copper bulk on one side of the sample set for holding the sample plates. Taking together, the anisotropic background and sample volume issue, we can qualitatively understand the anisotropic intensity of the magnetic excitations in the $[H, K]$ plane. In principle, the intensity of the magnetic excitations should exhibit six-fold rotational symmetry. Moreover, additional peaks appear close to $(0, -0.5)$, $(-0.5, 0.5)$, and $(0, 0.5)$ in (a). Since they appear close to half of the first three nuclear peaks $(0, -1, 0)$, $(-1, 1, 0)$, $(0, 1, 0)$ and are also present at 10 K with the same intensity, we attribute it to coherent nonmagnetic structural scattering.

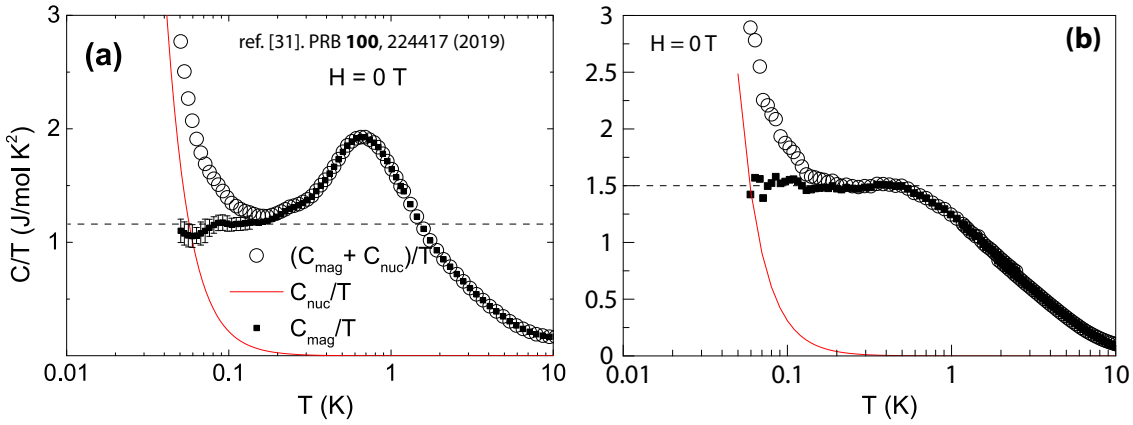


FIG. 9. Temperature-dependence of zero-field heat capacity for $NaYbSe_2$ and the subtraction of the low-temperature nuclear contribution $C_{\rm nuc}$/T. The open circles, solid squares, and red curves are $(C_{\rm mag}+C_{\rm nuc})$/T, $C_{\rm mag}$/T, and the fitting of $C_{\rm nuc}$/T. The data in (a) are reproduced from ref. [31] of the main text and (b) from our results (Fig. 1(e) in the main text). The magnetic contribution $C_{\rm mag}$ for both samples in (a) and (b) exhibit a constant region below 0.2 K.

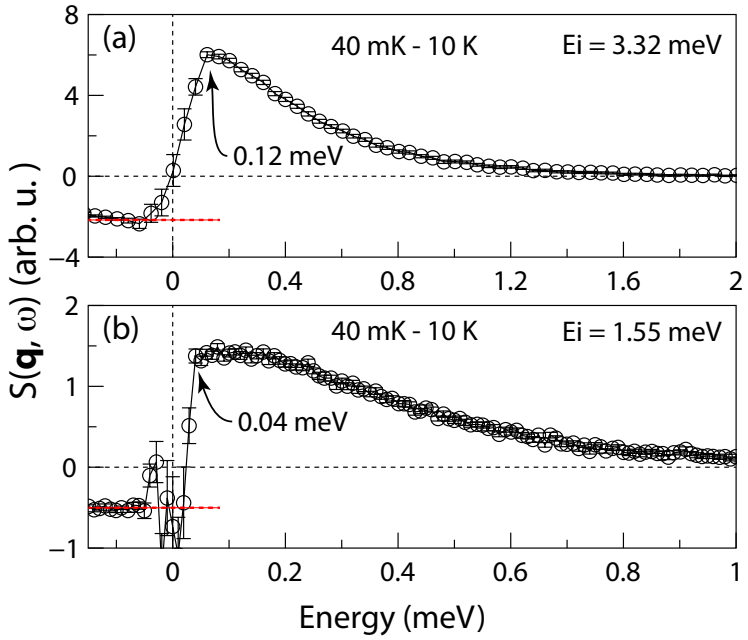


FIG. 10. The intensity difference between the spin excitations measured at K_1 point with 40mK and 10K. Data in (a) is collected with $E_i = 3.32$ meV and (b) with $E_i = 1.55$ meV. The black arrows mark the lowest energies resolved with undiminished intensity. The red dashed lines arise from the increase of the background scattering at $T = 10$K. If we assume the background increase with temperature is energy independent and subtract this increase from the 10 K data, the spectral weight difference shown above will be shifted upward constantly and become finite at $E \geq 0$.